

Influence of hydrogen on electron-phonon coupling and intrinsic electrical resistivity in zirconium: A first-principles study

Qicheng Tang,* L. A. Svyatkin, and I. P. Chernov

Tomsk Polytechnic University, Prospekt Lenina 30, 634050 Tomsk, Russia

(Dated: March 12, 2019)

We present a first-principles study of the electron-phonon coupling and temperature dependence of intrinsic electrical resistivity in the zirconium-hydrogen system with various concentrations of hydrogen. By means of density functional theory and density functional perturbation theory, the Eliashberg function $\alpha^2F(\omega)$, Eliashberg transport function $\alpha_{tr}^2F(\omega)$ and their strength electron-phonon coupling constant λ and transport constant λ_{tr} were calculated. By solving Boltzmann equation in the lowest-order variational approximation, we got the temperature dependence of intrinsic electrical resistivity. The present calculated hydrogen concentration dependence of electrical resistivity in zirconium is in good agreement with experimental results, where a reduction of electrical resistivity at a high concentration $H/Zr > 1.5$ was observed. We analyzed the relevance of the reduction in electrical resistivity with change of ratio c/a , it's found that the hydrogen concentration, where the resistivity starts to decrease, is very close to the concentration of $\delta - \varepsilon$ phase transition. As an example, we investigated the influence of values of c/a on behaviors of system ZrH_2 , and we show the relevance of the reduction in electrical resistivity with the tetragonal distortion which is related to structural stability of system.

PACS numbers: 63.20.Kr, 64.70.Kb, 71.15.Mb, 71.20.Be, 72.10.Di, 72.15.-v

I. INTRODUCTION

The feature of interaction between metal and hydrogen has extensively been studied over many years.¹⁻³ These studies have both practical and theoretical significances in many different areas, like energy storage, superconductor and other modern technologies. The interaction between metal and hydrogen is strong and leads to the change of mechanical, transport, magnetic and other properties of metal. The change of physical properties is related to renormalization of electron, phonon structures and electron-phonon coupling spectrum. Interest in electron-phonon coupling of metal-hydrogen systems was initiated about half a century ago by the discovery of a high increase of superconducting critical temperature due to hydrogen absorption in thorium⁴ and in palladium⁵. The describing of electron-phonon coupling is not only important for superconductivity, but also for transport properties of metal. By means of measuring electrical resistivity of material, the information of impurities and defects in material can be obtained. An accurate dataset of electrical resistivity for pure metal-hydrogen system can help us to analyze the impurity-character and defect-character scattering in real material. An interesting fact observed in experiment is the reduction of electrical resistivity in some hydrogen-metal systems at a very high hydrogen (H) concentration, like in palladium-hydrogen system is $H/Pd \approx 0.71$ at 300 K⁶, $H(D)/Pd \approx 0.75$ at 298 K⁷ and in zirconium-hydrogen system is $H/Zr \approx 1.68$ at 300 K. This phenomenon is still not explained by theoretical calculation.

In this work, we focus on the situation of the zirconium-hydrogen system. Zirconium-based alloys are extensively used for the fabrication of fuel cell shells for nuclear reactors, since zirconium (Zr) has a low thermal-

neutron absorption cross section. In this case, the atomic H is produced by decomposition of hydronium at a high temperature (about 600 K).⁹ The structural stability and mechanical properties of the Zr-H system are widely studied, a few experimental and calculational works showed that at a low H concentration, system has hexagonal close packed (HCP) structure and H atoms are located at tetrahedral (T) interstitial sites¹⁰⁻¹³. For Zr_4H_2 , the metastable state, which has a HCP structure with a low symmetry, was obtained by combining TEM experimental results and first-principles calculations¹⁴. It was also reported that the Zr_2H system has a face-centered cubic (FCC) structure in a high symmetry condition by calculation work¹⁰. At a high H concentration ($1 \leq x = H/Zr \leq 2$), the Zr-H system has a FCC or face-centered tetrahedral (FCT) structure^{11,15-18}. The transition from δ phase (FCC structure) into ε phase (FCT structure, $c < a$) is a focus of many research investigations^{16,18-22}, and the H concentration of phase transition is located at $x \geq 1.5$. It has been reported that there is a strong reduction in electronic density of states at Fermi level upon formation of the ε phase for ZrH_2 , to ~ 0.5 states/eV unit cell²², which leads to the $\delta - \varepsilon$ phase transition. The electron-driven mechanisms of $\delta - \varepsilon$ phase transition in Zr-H system with $1 \leq x \leq 2$ have been investigated in many works^{17,22-26}, but to our knowledge there is still no report regarding the relevance of the transition with electron-phonon coupling. The reason for why we consider a relation between electron-phonon coupling and the $\delta - \varepsilon$ phase transition, is that the transition H concentration is close to the concentration where the electrical resistivity starts to decrease with increasing of hydrogen concentration. In fact, there are a few works^{7,27} for palladium-hydrogen system, pointed out the relevance of the phase transition and reduction of electrical resistivity at a high H concentration. Meanwhile, Zr-H system is

still a metallic system in principle, which means that the main contribution of electrical resistivity of Zr-H system is still electron-phonon scattering.

The purpose of this paper is to present a first-principle study regarding the influence of H on electron-phonon coupling and intrinsic electrical resistivity in Zr. We calculated the situation for $\text{ZrH}_{0.5}$, ZrH , $\text{ZrH}_{1.25}$, $\text{ZrH}_{1.5}$, $\text{ZrH}_{1.75}$, ZrH_2 and pure Zr to show the H concentration dependence of electrical resistivity in Zr-H system. The electron-phonon coupling was analyzed by means of Eliashberg function $\alpha^2F(\omega)$ and Eliashberg transport function $\alpha_{tr}^2F(\omega)$. To clarify the relevance between the $\delta - \varepsilon$ phase transition and reduction of electrical resistivity, we investigated the changes of electron-phonon coupling through the tetragonal distortion for ZrH_2 as an example. In addition, for Zr_2H we compared the situation of HCP and FCT structure, and we show the results of structural stability. The paper is structured as follows. The methodology and computation details in this work are given in Sec. II. In Sec. III, we present computational results and discuss of the structural transformation, intrinsic electrical resistivity, electron-phonon interaction and Fermi surface nesting in Zr-H system. Summary and conclusions are drawn in Sec. IV.

II. COMPUTATIONAL DETAILS

In our work, all calculations are from first principles within density functional theory (DFT) and density functional perturbation theory (DFPT) as implemented in ABINIT²⁸ code. Our calculations have been carried out using the optimized norm-conserving Vanderbilt pseudopotential method (ONCVSP)²⁹ with the generalized gradient approximation of Perdew, Burke and Ernzerhof (GGA-PBE)³⁰ for the exchange and correlation functional. The cut-off energy for plane wave basis was set to 30 Ha in the dynamical calculation (structural optimization and relaxation) and 40 Ha in the static calculation (electronic structure calculation and linear response calculation). For a metallic occupation achievement, the temperature smearing method of ‘‘cold smearing’’³¹ with a broadening of 0.001 Ha (about 316 K) was adopted, and the cut-off energy of smearing function was set to 0.5 Ha. For structural optimization, the Broyden-Fletcher-Goldfarb-Shanno minimization (BFGS)³² was adopted.

The present calculations have been performed for systems $\text{ZrH}_{0.5}$, ZrH , $\text{ZrH}_{1.25}$, $\text{ZrH}_{1.5}$, $\text{ZrH}_{1.75}$, ZrH_2 and pure Zr. In our calculations we considered three possible structures: HCP, FCC, and FCT, and the H atoms all occupy T sites or all O sites. To select the ‘‘stable structures’’, We compared the total energy of system and got possible stable structures (with lowest total energy) as the ‘‘real structures’’. We have got the same optimized structure and relaxed H location as shown in literature^{10,14}. In addition, we have done the dynamical calculation for $\text{ZrH}_{0.5}$ in FCT structure with the H addition all at T or octahedral (O) sites. The supercell with 4

Zr atoms was adopted in the dynamical calculation, and the k-meshes were chosen as $13 \times 13 \times 4$ for HCP structure and $14 \times 14 \times 14$ for FCC, FCT structures while a supercell with 4 Zr atoms. In this part, the self-consistent calculation is terminated when the total energy change is less than 10^{-8} Ha and the maximal force is less than 10^{-4} Ha/Bohr.

In electronic structure calculations (including the calculation of band structure and electronic density of states (EDOS)) for ZrH_2 δ and ε phases, the k-meshes of $32 \times 32 \times 32$ and $30 \times 30 \times 34$ were adopted, respectively. In this part, the self-consistent loop of static calculations is terminated when the total energy change is less than 10^{-8} Ha, the maximal force is less than 10^{-5} Ha/Bohr, and the non-self-consistent calculations of band structure is terminated when the wavefunction squared residual $\langle \psi_{n\mathbf{k}} | (\hat{H} - E)^2 | \psi_{n\mathbf{k}} \rangle$ is less than 10^{-16} Ha². Here $|\psi_{n\mathbf{k}}\rangle$ is an electronic eigen-state with eigen-energy level $\varepsilon_{n\mathbf{k}}$ (crystal momentum \mathbf{k} and band index n), \hat{H} is the Hamiltonian operator, and $E = \langle \psi_{n\mathbf{k}} | \hat{H} | \psi_{n\mathbf{k}} \rangle$.

In linear response calculations, for pure Zr and ZrH the supercell with 2 Zr atoms was adopted, the k-mesh of $14 \times 14 \times 10$ and the q-mesh of $7 \times 7 \times 5$ were chosen. For $\text{ZrH}_{1.25}$, $\text{ZrH}_{1.5}$, $\text{ZrH}_{1.75}$ the supercell with 4 Zr atoms was adopted, the k-mesh of $14 \times 14 \times 14$ and the q-mesh of $7 \times 7 \times 7$ were chosen. For ZrH_2 we have used the unit cell, the k-mesh of $24 \times 24 \times 24$ and the q-mesh of $12 \times 12 \times 12$ were chosen. For $\text{ZrH}_{0.5}$, we calculated five conditions. The first (C1), second (C2) and third (C3) conditions all have the HCP structure. C1 is the optimized structure by present calculation, and the H location is the same as the S2 in literature¹⁴. In the C2 and C3, H atoms occupy the same T site in per unit cell. The fourth (C4) and five-th (C5) conditions are systems in FCT structure with the atomic H addition all in the T or O sites. C1 and C2 was calculated by using the supercell $1 \times 1 \times 2$ with 4 zirconium atoms, and other three conditions were calculated by using the supercell with 2 Zr atoms. The k-mesh of $14 \times 14 \times 6$, the q-mesh of $7 \times 7 \times 3$ were chosen for C1 and C2, and the k-mesh of $14 \times 14 \times 10$, the q-mesh of $7 \times 7 \times 5$ were chosen for C3, C4 and C5.

By means of DFPT within linear response method, the first-order perturbation potentials $\Delta_{qv}v$ for a phonon with frequency ω_{qv} (crystal momentum \mathbf{q} and branch index v) were calculated. Then they were used in the calculation of the electron-phonon matrix elements as $g_{mnv}(\mathbf{k}, \mathbf{q}) = \langle \psi_{n\mathbf{k}+\mathbf{q}} | \Delta_{qv}v | \psi_{n\mathbf{k}} \rangle$. More details about the theoretical methods can be found in the review by Feliciano³³. For the calculation of electron-phonon matrix elements, the self-consistent calculations of ground-state are terminated when the wavefunction squared residual is less than 10^{-24} Ha², the self-consistent calculations of first-order perturbation potential is terminated when the potential residual is less than 10^{-18} Ha, and the non-self-consistent calculations of electron-phonon matrix elements are terminated when the wavefunction

squared residual is less than 10^{-24} Ha².

The Eliashberg function³⁴, which measures the contribution of phonon with frequency ω on scattering processes of electrons at the Fermi level, was calculated in terms of the phonon linewidths γ_{qv} by electron-phonon matrix elements,

$$\alpha^2 F(\omega) = \frac{1}{2\pi N(\varepsilon_F)} \sum_{qv} \sum_{mnk} \frac{\gamma_{qv}}{\omega_{qv}} \delta(\hbar\omega - \hbar\omega_{qv}), \quad (1)$$

where $N(\varepsilon_F)$ is the EDOS per atom and spin at the Fermi level ε_F . The linewidth is written as follows:

$$\gamma_{qv} = 2\pi\omega_{qv} \sum_{mnk} |g_{mn\nu}(\mathbf{k}, \mathbf{q})|^2 \delta(\varepsilon_{n\mathbf{k}} - \varepsilon_F) \delta(\varepsilon_{m\mathbf{k}+\mathbf{q}} - \varepsilon_F). \quad (2)$$

The strength of $\alpha^2 F(\omega)$ is described by parameter

$$\lambda = 2 \int_0^\infty \frac{d\omega}{\omega} \alpha^2 F(\omega), \quad (3)$$

which is called the electron-phonon coupling constant.

For calculation of transport properties, the tetrahedron smearing method³⁵ was adopted. Electron-phonon scattering has a dominant contribution to the electrical resistivity of metallic systems except for the very low-temperature region where the impurity and electron-electron scattering are important. The Eliashberg transport function³⁶, which is used to describe the influence of the electron-phonon scattering on transport properties, compares to Eliashberg function additionally considers the efficiency factor of electronic transport $\eta_{\mathbf{k},\mathbf{q}}^{mn\nu}$, is calculated as following

$$\alpha_{tr}^2 F(\omega) = \frac{1}{N(\varepsilon_F)} \sum_{qv} \sum_{mnk} |g_{mn\nu}(\mathbf{k}, \mathbf{q})|^2 \delta(\varepsilon_{n\mathbf{k}} - \varepsilon_F) \times \delta(\varepsilon_{m\mathbf{k}+\mathbf{q}} - \varepsilon_F) \delta(\hbar\omega - \hbar\omega_{qv}), \quad (4)$$

where an efficiency factor $\eta_{\mathbf{k},\mathbf{q}}^{mn\nu} = \frac{\mathbf{v}_{n\mathbf{k}} \cdot \mathbf{v}_{m\mathbf{k}+\mathbf{q}} \cdot \mathbf{v}_{n\mathbf{k}}}{\langle v^2 \rangle}$ has been introduced in terms of the electron velocity $\mathbf{v}_{n\mathbf{k}}$ in the state $|\psi_{n\mathbf{k}}\rangle$, and here $\langle v^2 \rangle$ is the average square of the Fermi velocity. The strength of $\alpha_{tr}^2 F(\omega)$ is described by parameter

$$\lambda_{tr} = 2 \int_0^\infty \frac{d\omega}{\omega} \alpha_{tr}^2 F(\omega), \quad (5)$$

which is called transport constant. For normal metal, the electrical resistivity can be calculated by solution of the Boltzmann equation in the lowest-order variational approximation (LOVA), and written in terms of $\alpha_{tr}^2 F(\omega)$ as follows

$$\rho(T) = \frac{\pi\Omega k_B T}{N(\varepsilon_F) \langle v^2 \rangle} \int_0^\infty \frac{d\omega}{\omega} \frac{x^2}{\sinh^2 x} \alpha_{tr}^2 F(\omega), \quad (6)$$

where $x = \hbar\omega/(2k_B T)$ and Ω is the volume of calculated cell.

To make it simple, we use the representations of HCP(T), FCC(T), and FCC(O) to signify the three calculated situations in following text, tables, and figures. For example, the HCP structure Zr with additions of H atoms at T sites is represented as HCP(T).

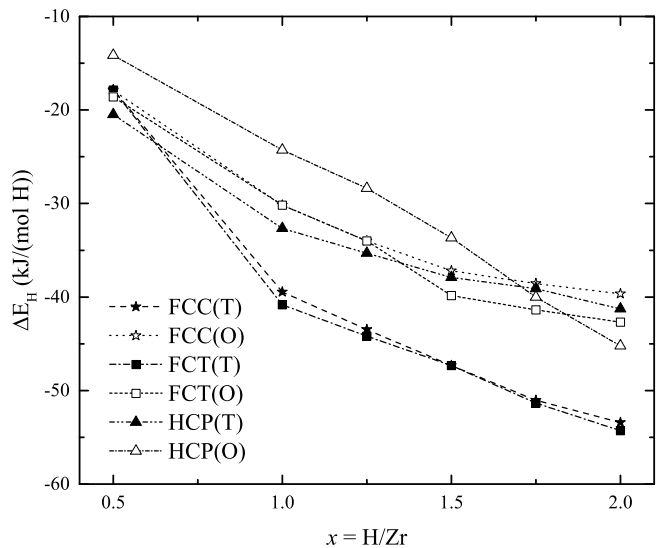


FIG. 1. The energy of hydrogen solution for Zr-H system with various hydrogen concentration.

III. RESULTS AND DISCUSSION

A. Structure of Zr-H system

In present calculations, the effect of hydrogen on the crystal structure in various Zr-H systems was investigated. To find out the effect of H on structural stability, the energy of H solution for various Zr-H systems was calculated according to the following formula

$$\Delta E_H = \frac{E_{Zr_n H} - nE_{Zr} - \frac{1}{2}E_{H_2}}{n+1}, \quad (7)$$

where $E_{Zr_n H}$, E_{Zr} and E_{H_2} are total energies of $Zr_n H$, pure HCP Zr (ground state) and H_2 molecule, respectively. Consequently, the ΔE_H of various ZrH_x systems as a function of H concentration are shown in Fig. 1. It is energetically most advantageous for the ZrH_x system to have a HCP(T) lattice structure at a hydrogen concentration of $x = 0.5$ and a FCC(T) structure at a hydrogen concentration of $1 \leq x \leq 2$. At a concentration of $1.5 \leq x \leq 1.75$, the dissolution energy of H in Zr with a FCT structure exceeds its dissolution energy in Zr with a FCC structure by an amount not exceeding 0.1 eV/atom H. As a result, under perturbation (for example, under the influence of radiation or high temperatures), the ZrH_x system can pass from the FCT structure to the FCC structure. It also can be seen that the H concentration dependence of ΔE_H is linear in the ranges $0 \leq x \leq 1$ and $1 \leq x \leq 2$, respectively. Through a linear fitting, the slope of function is -41.7 kJ/(mol H) with $R^2=0.9996$ in range $0 \leq x \leq 1$, and -48.6 kJ/(mol H) with $R^2=0.9657$ in range $1 \leq x \leq 2$ were obtained, which agree well with the experimental values³⁷ of -41 and -52 kJ/(mol H), respectively.

One should be pointed out that the HCP(T) struc-

TABLE I. Lattice parameters (a and c) for calculated ZrH_x systems with H located all at T sites or all at O sites.

System	Structure	a (Å)	c (Å)	c/a	Method	Reference
Pure zirconium	HCP	3.2346	5.1678	1.5976	GGA	Present work
		3.2317	5.1476	1.5928	Exp. (298K)	11
		3.213	5.159	1.605	GGA	10
		3.23	5.18	1.60	GGA	38
Zr_2H	HCP(T), C1	3.2603	5.3962	1.6551	GGA	Present work
		3.3	5.145	1.56	Exp. (293K)	14
		3.313	5.549	1.675	GGA	10
	HCP(T), C2(C3)	3.2433	5.4892	1.6925	GGA	Present work
		3.26	5.447	1.671	GGA	10
	FCT(T), C4	4.7597	4.4595	0.9369	GGA	Present work
		4.676			GGA	10
	FCT(O), C5	4.4334	4.8431	1.0924	GGA	Present work
4.575				GGA	10	
ZrH	FCT(T)	4.5754	5.0045	1.0938	GGA	Present work
		4.5957	4.9686	1.081	Exp. (293K)	2
		4.61	5.04	1.093	GGA	26
$\text{ZrH}_{1.25}$	FCT(T)	4.6130	5.0252	1.0894	GGA	Present work
		4.79	5.20	1.086	GGA	26
$\text{ZrH}_{1.5}$	FCT(T)	4.7276	4.8874	1.0338	GGA	Present work
		4.65	4.96	1.067	Exp. (320K)	18
		4.62	4.83	1.046	GGA	26
$\text{ZrH}_{1.75}$	FCT(T)	4.9585	4.4651	0.9005	GGA	Present work
		4.9087	4.5220	0.9212	Exp. (118K)	17
		4.97	4.47	0.899	GGA	26
ZrH_2	FCT(T)	5.0053	4.4106	0.8812	GGA	Present work
		4.9808	4.4336	0.8901	Exp. (108K)	17
		4.975	4.447	0.894	Exp. (294K)	16
		4.982	4.449	0.893	Exp. (320K)	18
		5.021	4.432	0.883	GGA	22
	FCC(T)	4.8089			GGA	Present work
		4.817			GGA	22
		4.82			GGA	38
		4.804			LDA	24

ture for $\text{ZrH}_{0.5}$, presented in Fig. 1, is the condition C1, which has a lowest energy in three conditions (C1-3) with HCP(T) structure. The conditions C2, C3 have a total energy close to the conditions C4, C5 with a FCT lattices, and the difference is less than 0.0004 eV/Zr atom, which is the same energy from an environment temperature less than 5 K. It is clear to see that the size of supercell using in calculation has a meaning to structural optimization. When the small supercell (with 2 Zr atoms) was used, the energetic difference between HCP and FCT is small, but when the bigger supercell (with 4 Zr atoms) was used, the energetic difference of FCT with HCP is about 6.6 kJ/(mol H). The result is in good agreement with the previous result¹⁴.

In Table I, we show a comparison of the present cal-

culated structural parameters (a and c) for pure Zr, $\text{ZrH}_{0.5}$, ZrH, $\text{ZrH}_{1.25}$, $\text{ZrH}_{1.5}$, $\text{ZrH}_{1.75}$ and ZrH_2 with previous calculations and experimental data available in literature^{2,10,11,14,16-18,22,38}. The present calculations predict a c/a ratio for pure Zr, ZrH, $\text{ZrH}_{1.25}$, $\text{ZrH}_{1.5}$, $\text{ZrH}_{1.75}$ and ZrH_2 that the difference with experimental data is less than 3%, and the present value of lattice parameters for these systems is also in a good agreement with previous calculations and experimental data. For ZrH_2 with FCC structure, the difference of lattice parameter in present calculations with previous calculations is less than 0.3%. In addition, the structural difference between C1 and C2 for $\text{ZrH}_{0.5}$ has been observed. The present results for C1 and C2 show that the lattice volume of C2 is 1.0067 times that of C1, and the ratio c/a

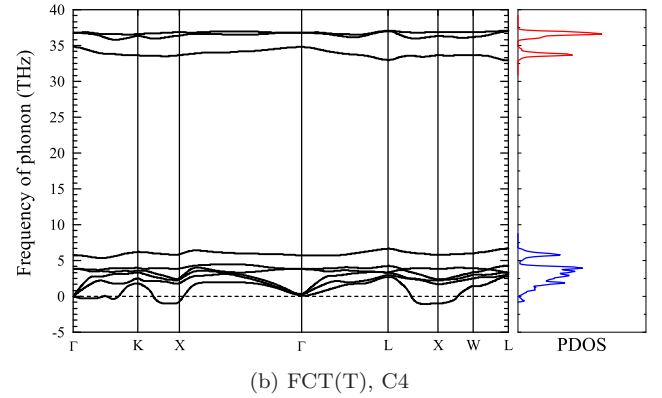
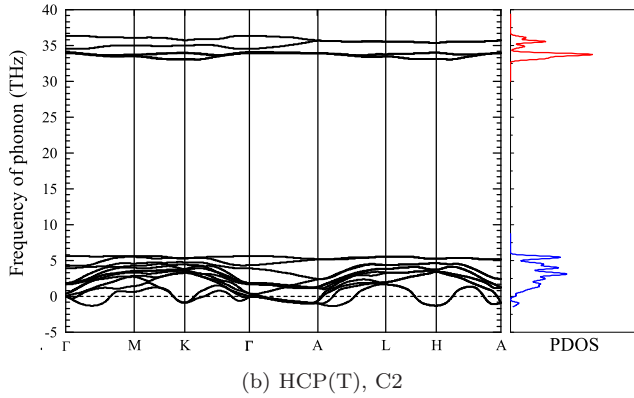
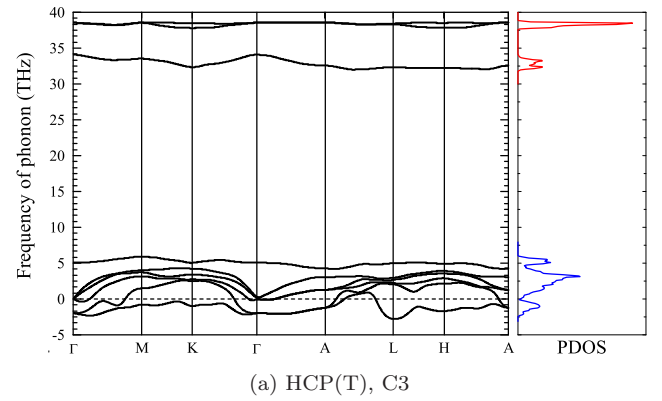
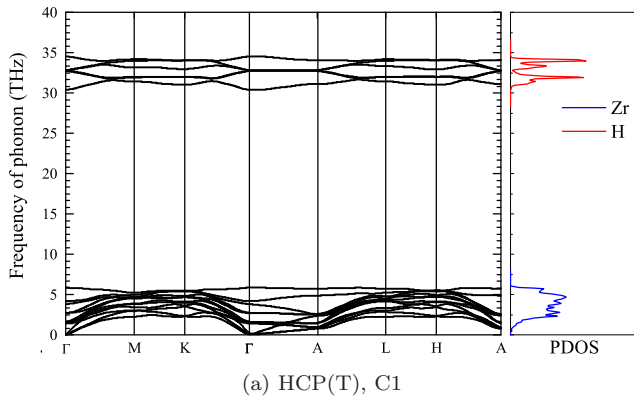


FIG. 2. The phonon spectrum for Zr_2H low symmetry conditions C1 and C2 with HCP(T) structure.

of C2 is also larger than C1. For the condition of Zr_2H , the predicted lattice volume in present calculations for FCT structure that ranges within 1 – 2% of the calculation results¹⁰, but we additionally considered the tetragonal distortion of system. We conclude that we found very good agreement of the calculated lattice parameters in the present work with the previous calculations and experimental data for the Zr-H system. For the high H concentration condition ($1 \leq x \leq 2$), we got a $\gamma(c > a) - \delta - \varepsilon$ phase transition process, and the H concentration for appearing of $\delta - \varepsilon$ phase transition is $x = 1.57$, which is similar to the experimental results $x = 1.6$ ¹⁸. It has been observed that the ratio c/a decreases with the increasing of H concentration in Zr, as in experiments^{17,18}.

In addition, we analyzed structural stability for $ZrH_{0.5}$ in five conditions (C1-C5) by calculated phonon spectrum. In Figure 2, we show phonon spectrum for the low symmetry conditions C1 and C2. It is clear to see that the H location in Zr has a meaning to structural stability of Zr-H system, C2 has the imaginary phonon frequency but C1 does not. The H-character optical phonon modes in C2 are higher than in C1 about 3 THz, so that the gap between optical and acoustical modes in C2 also larger than in C1. It means that the H location also has the influence on effective mass of its phonon. In Figure 3, we show phonon spectrum for the high symmetry conditions

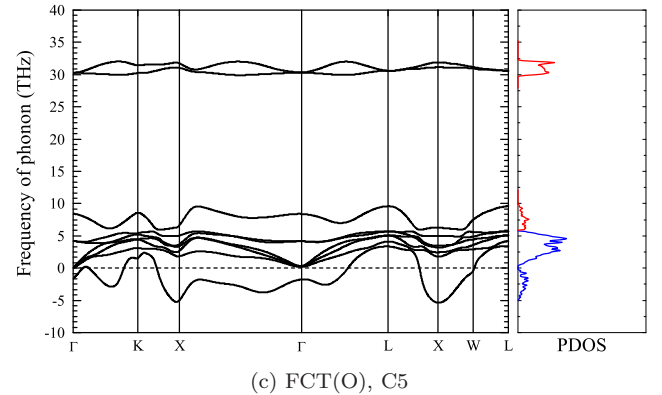


FIG. 3. The phonon spectrum for Zr_2H high symmetry conditions C3, C4, and C5 with HCP(T), FCT(T), and FCT(O) structures, respectively.

C3, C4 and C5. Although the C5 has the lowest total energy in the three conditions, the phonon spectrum shows that C5 has the largest imaginary phonon frequency of -5.41 THz which is located at X point. It should be noticed that the gap between optical and acoustical phonon modes is small than 0.15 THz, it means that the acoustical Zr-character phonons can make transitions into optical phonons by a low energy equivalent to temperature 7.2 K. Thus, we conclude that C5 is an instable state even at a very low temperature. It is also clear to see that C4 is much more stable than C5, and the difference only between C4 and C5 only from the H location in Zr.

B. Electron-phonon coupling, electrical resistivity of Zr-H system

As the beginning of the discussion about the electron-phonon coupling and electrical resistivity of Zr-H system, we present the temperature dependence of electrical resistivity of pure Zr and the H concentration dependence of electrical resistivity in Fig. 4 and Fig. 5, respectively. As shown in Figure 4, our calculational results for $[\bar{1}2\bar{1}0]$ and $[10\bar{1}0]$ directions are close to the experimental data³⁹. Therefore, as shown in Figure 5, we choose the average value of electrical resistivity in $[\bar{1}2\bar{1}0]$ and $[10\bar{1}0]$ directions as the calculational results for pure Zr and ZrH_{0.5} system (both have HCP structure). For zirconium hydrides we also choose an average value of electrical resistivity in different directions as the calculational results, for two-atom supercells the directions are $[1\bar{1}0]$ and $[110]$, for four-atom supercells the directions are $[100]$, $[010]$ and $[001]$. It can be seen that our results of H concentration dependence are also in good agreement with experimental data⁸ at 300 K. We also present the H concentration dependence at a typical work temperature of nuclear reactor 650 K, unfortunately, to our knowledge there is no experiment data for this temperature. It should be noticed that the trend of $\rho(x)$ persists at different temperatures, but it is sharper at a higher temperature as shown in Fig. 5, because the lattice vibration is stronger at a higher temperature. In present calculations the low temperature condition was not calculated, because the electron-phonon scattering is not the main contribution of transport properties of system at a low temperature, where the effects of electron-electron scattering, size effects, impurity scattering, etc., are considerable. At a very high temperature (higher than 800 K), the difference between calculated and experimental results becomes considerable with increasing temperature. This situation has been caused by two factors. The main factor is that the system transforms from α phase (with a HCP structure) into β phase (with a body-centered cubic (BCC) structure) with the increasing of temperature¹¹. The another factor is that in present work the electron-phonon interaction was calculated within the harmonic approximation which doesn't work at an elevated temperature. It should be pointed out that the temperature 650 K cannot lead to a phase transition of the Zr-H system, and it is also not such an elevated temperature for harmonic approximation. Thus, we conclude that the present calculation results of the electron-phonon coupling and electrical resistivity in the Zr-H system are credible, and have a practical significance.

Let's focus on the H concentration dependence $\rho(x)$, as shown in Fig. 5, the reduction in ρ at a high H concentration ($x > 1.5$) has been observed both in previous experiment and present calculations. The calculational result for ZrH₂ $\rho = 27.52 \mu\Omega \text{ cm}$ is similar to the experimental data⁸ for ZrH_{1.96} $\rho = 26.7 \mu\Omega \text{ cm}$, and both results show that ZrH₂ is a better electrical conductor than pure Zr. In present calculations we got the H concentration x_c ,

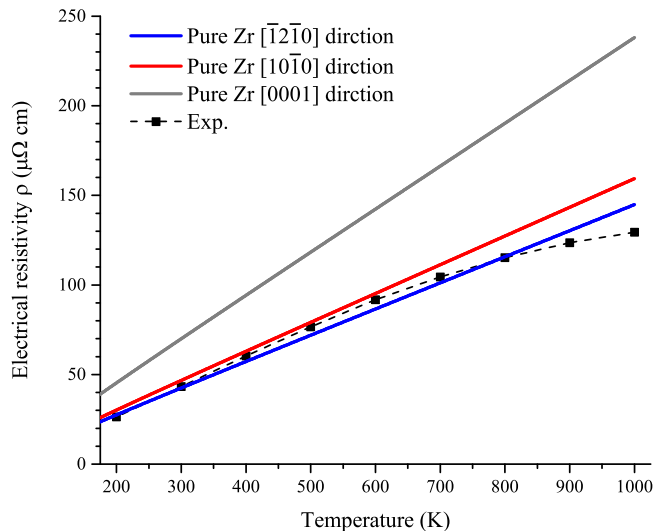


FIG. 4. A comparison of present calculational temperature dependence of electrical resistivity $\rho(T)$ of pure Zr with experimental data³⁹.

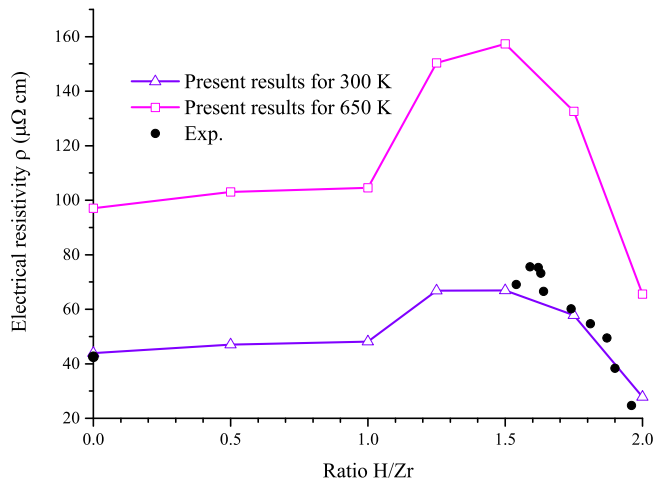
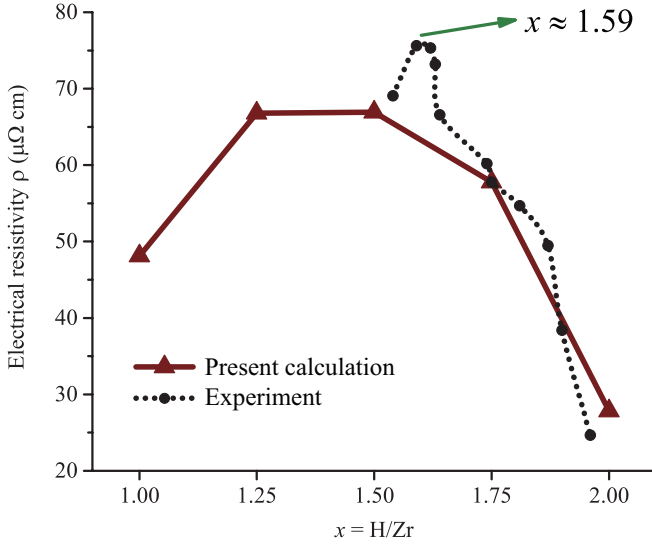
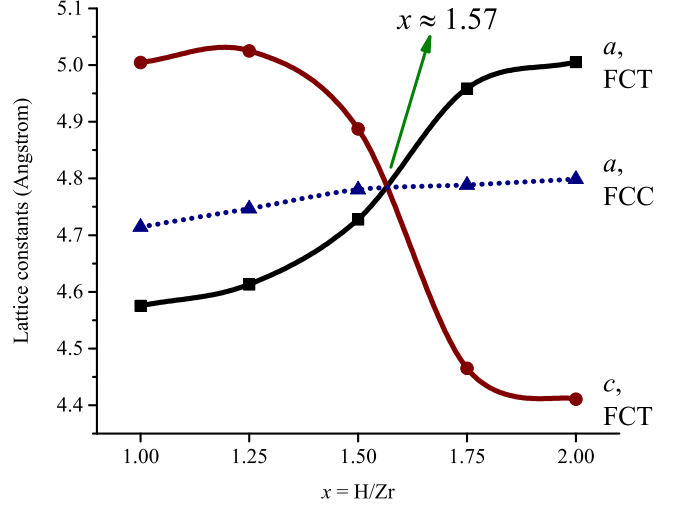


FIG. 5. A comparison of present calculational hydrogen concentration dependence of electrical resistivity $\rho(x)$ of Zr-H system with experimental data⁸.

where the resistivity starts to decrease with the increasing of H concentration, is in the range from 1.5 to 1.75. This result is in agreement with experiment⁸, where the results showed the x_c is in the range from 1.54 to 1.62. Interestingly, the concentration x_c is close to the concentration for transition from δ phase to ϵ phase. Hence, it's natural to consider the relevance of reduction in ρ with the $\delta - \epsilon$ phase transition. It should be noticed that the only difference between δ and ϵ phases is the value of c/a . In Figure 6, we present a comparison of H concentration dependence of electrical resistivity and lattice constants for zirconium hydrides. As shown in Figure 6b, the value of a increases and c decreases with increasing H concentration in Zr, i.e. value of c/a decreases with increasing



(a) Dependence of electrical resistivity on H concentration in zirconium for hydrides zirconium at 300 K



(b) Dependence of lattice constants on H concentration in zirconium for hydrides zirconium with FCC or FCT structures

FIG. 6. A comparison of H concentration dependence of electrical resistivity and lattice constants for hydrides zirconium.

value of x . It is clear to see that the concentration x_c is close to the concentration $x \approx 1.57$, where $c = a$. Thus, we can conclude that there is a relevance of reduction in ρ with tetragonal distortion of FCC lattice, later we will discuss the details in Sec. III C.

Furthermore, we focus on the electron-phonon coupling in the Zr-H system. The calculated Eliashberg function $\alpha^2 F(\omega)$, Eliashberg transport function $\alpha_{tr}^2 F(\omega)$ and their strength electron-phonon coupling constant $\lambda(\omega)$ and transport constant $\lambda_{tr}(\omega)$ for zirconium dihydrides and pure zirconium are show in Fig. 7. The calculational results show that the Zr-H system has the characteristics of transition metals. The value of $\lambda = 0.54$ for pure zirconium shows a not weak electron-phonon coupling which is general for transition metals, owing to the large effective mass of d-electrons in transition metals. In practice, the agreement between calculated results and experimental data of electrical resistivity can be a verify of authenticity for calculated $\alpha_{tr}^2 F(\omega)$, so we conclude that the present calculated electron-phonon coupling spectrum are credible. We show that the Eliashberg function and Eliashberg transport function have a common shape as in a normal condition⁴⁰, where the efficiency factor $\eta_{\mathbf{k},\mathbf{q}} = \frac{v_{n\mathbf{k}}^2 - v_{m\mathbf{k}+\mathbf{q}} \cdot v_{n\mathbf{k}}}{(v^2)}$ from electronic velocity only has a small contribution on electron-phonon scattering process for a metallic system, the ratio $\lambda_{tr}/\lambda \approx 1$ also shows that. In particular, the efficiency factor $\eta_{\mathbf{k},\mathbf{q}}$ gives a preferential weight from the backscattering process. The ratio λ_{tr}/λ is close to 1 for stable structures, the minimum is the ratio $\lambda_{tr}/\lambda = 0.83$ for $\text{ZrH}_{1.25}$, and the maximum is the ratio $\lambda_{tr}/\lambda = 1.17$ for $\text{ZrH}_{1.75}$.

It should be noticed that the $\text{ZrH}_{1.25}$ is the only one $\lambda > \lambda_{tr}$ in the situations with a stable structure, and the

value of λ is also bigger than other situations. First, the big value of λ shows a strong electron-phonon coupling in $\text{ZrH}_{1.25}$ system, and it can explain the sudden rise of ρ for $\text{ZrH}_{1.25}$ system as shown in Fig. 5. Second, the electron backscattering weakens the strong coupling, it seems like that the system spontaneously defies the strong coupling. The same behavior has been observed in the two unstable ZrH_2 systems (with $c/a = 0.94$ and $c/a = 1$). Specially, for δ phase of ZrH_2 there is a significant difference between $\alpha^2 F(\omega)$ and $\alpha_{tr}^2 F(\omega)$ due to the backscattering of electrons, which may cause a strong Fermi surface nesting⁴¹ and a phase transition. It's clear to see that with decreasing value of c/a the values $\lambda = 3.769$ and $\lambda_{tr} = 1.212$ drop to $\lambda = 0.188$ and $\lambda_{tr} = 0.213$, the large value of $\lambda/\lambda_{tr} = 3.11$ drops to 0.88. This means that through tetragonal distortion the electron-phonon coupling becomes weaker and the strong Fermi surface nesting of δ phase is receded, and the weak electron-phonon coupling in ε phase ZrH_2 can explain why ZrH_2 is a better conductor than pure Zr.

The contribution of electron-phonon scattering from H atoms is also an interesting topic. In present calculations, it is found that the H-character optical phonons have a small contribution on λ and λ_{tr} , and Zr-character acoustic phonon modes have the largest contribution on λ , between 89% and 98% of the total for Zr-H systems with various H concentration. The reason may be the strong chemical bond between H and Zr, and the vibration modes of H are limited in a small scale by the strong chemical bond, it also can explain why the harmonic approximation well works in present calculation for Zr-H system by the low contribution of H on electron-phonon coupling. The ratio of $\lambda_{\text{H}}/\lambda$ for ZrH , $\text{ZrH}_{1.25}$, $\text{ZrH}_{1.5}$, $\text{ZrH}_{1.75}$ and ZrH_2 is 2%, 3%, 10%, 7% and 11%, respec-

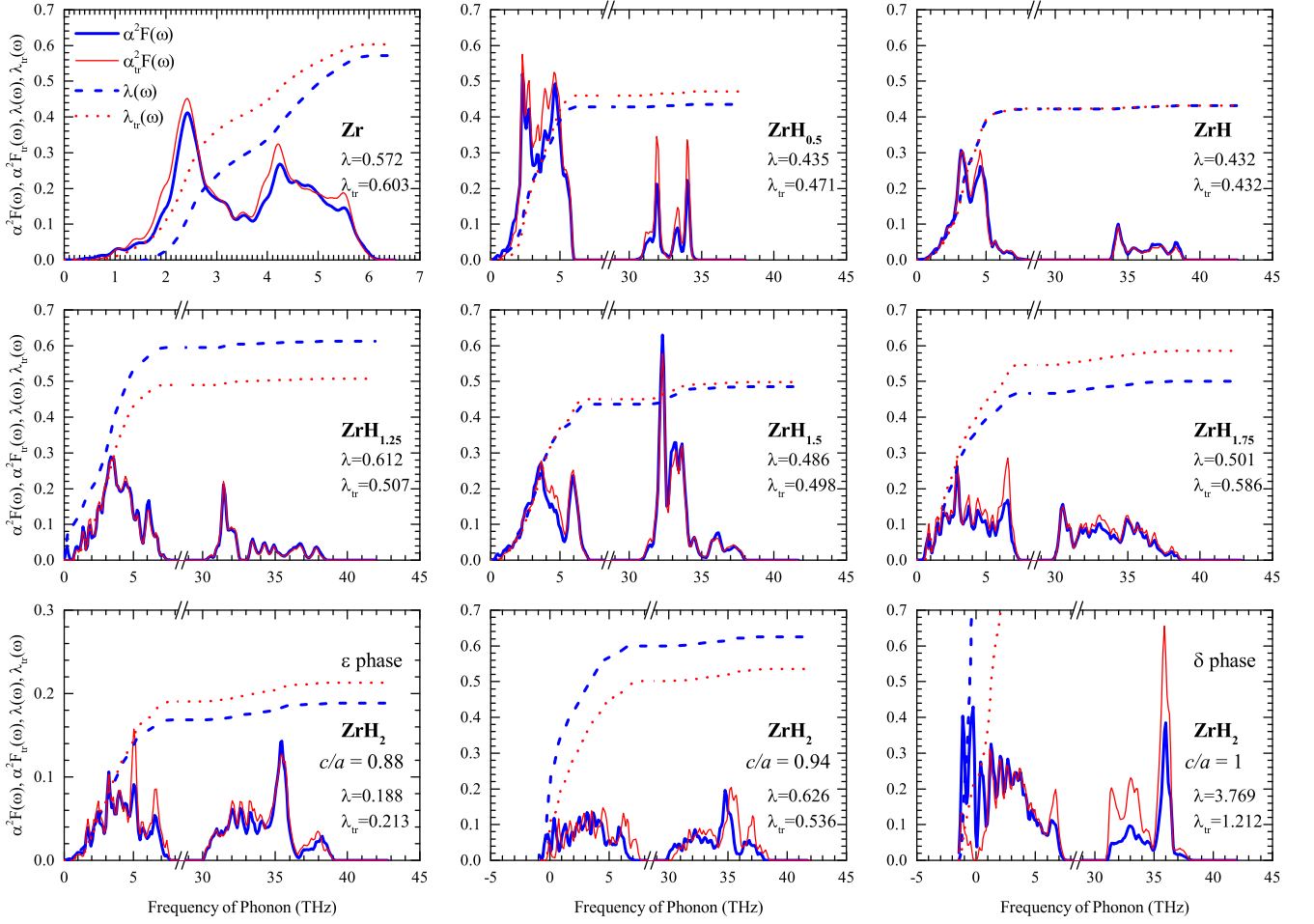


FIG. 7. The calculated Eliashberg function $\alpha^2 F(\omega)$, Eliashberg transport function $\alpha^2 F_{tr}(\omega)$ and their strength electron-phonon coupling constant λ and transport constant λ_{tr} for pure zirconium, $ZrH_{0.5}$, ZrH , $ZrH_{1.25}$, $ZrH_{1.5}$, $ZrH_{1.75}$ and ZrH_2 .

tively. It can be seen that the H-character optical phonon modes are getting to play a dominate role in electron-phonon coupling with the increasing of H concentration, and the reduction of λ_H/λ from $ZrH_{1.5}$ to $ZrH_{1.75}$ can be viewed as a result of $\delta - \varepsilon$ phase transition. We conclude that the H-concentration dependence of electron-phonon coupling in Zr-H system is driven by effect of H on acoustic phonon modes, i.e. lattice structural modification due to H, is the main contribution to the change of electron-phonon coupling strength. In particular, the system has a limited robustness, the strong chemical bond between Zr and H restricts the scale of H vibration modes. When the vibration is so strong that cannot be holed in system, the robustness of system refuses the strong vibration, and leads to a phase transition. If we focus on electrons, it is the same picture that the strong Fermi surface nesting can cause the structural transition of system. Thus, it is reasonable to estimate that there is a deep connection between the tetragonal distortion of FCC structure ($\delta - \varepsilon$ phase transition) and the reduction of electron-phonon coupling strength and electrical resistivity, we show this in the follows.

C. Electron-phonon driven phase transition and reduction of electrical resistivity: An example of ZrH_2

In this section we will in detail discuss the influence of tetragonal distortion of FCC structure on behaviors of ZrH_2 as an example. As we said, the instability of FCC structure plays a important role in reduction of electrical resistivity. There are three indications of the structural instability of δ phase: high pick of EDOS, imaginary phonon frequency and extremely high value of Fermi surface nesting factor, and they are corresponding to the electron-, phonon-, and electron-phonon- driven mechanism of tetragonal distortion in Zr-H system. As the beginning, we reveal the mechanism of tetragonal distortion in terms of electronic structures. Many researches on the electron-driven mechanism of $\delta - \varepsilon$ phase transition for ZrH_2 have been reported as we said in introduction. There are three main electron-driven mechanisms, first is the splitting of the bands at Fermi level in the $\Gamma - L$ direction due to Jahn-Teller effect^{17,21,22,24}, second is the reduction of $N(\varepsilon_F)$ by a shift in energy of the band along

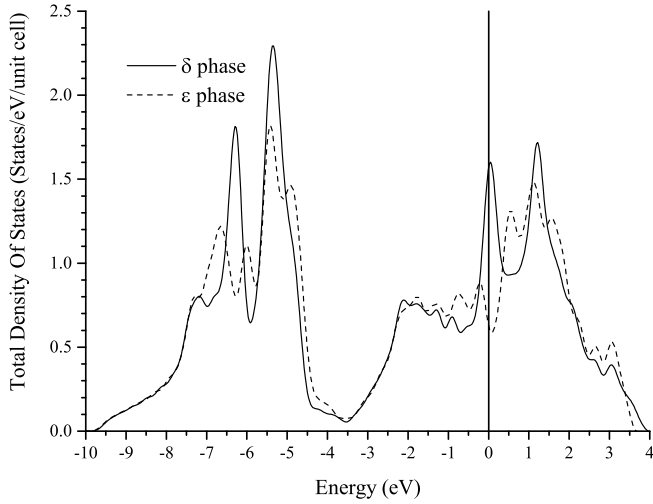


FIG. 8. The total EDOS in ZrH_2 δ and ϵ phases, and the Fermi level is set to the zero point.

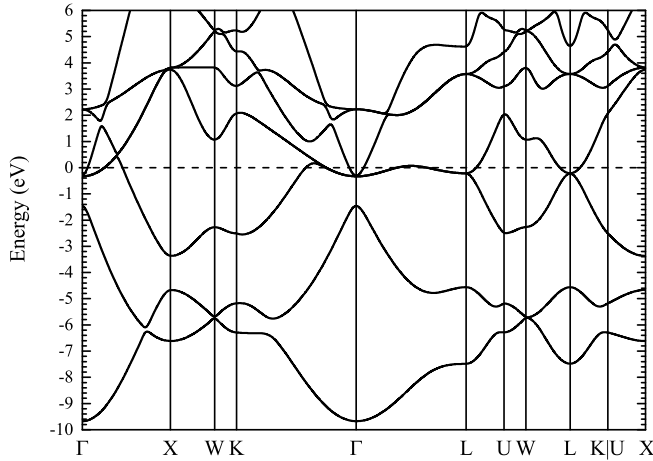


FIG. 9. The electronic structure of ZrH_2 δ phase.

the $\Gamma - K$ direction^{20,22}, and the third is the van Hove singularity in the $\Gamma - X$ direction²². In present work, we also calculated the electronic structure of ZrH_2 δ phase, and signs of the three mechanism were observed as shown in Fig. 9. The key point of these mechanism is that they lead to the reduction in $N(\epsilon_F)$ from δ phase to ϵ phase. In Figure 8, we show a comparison of EDOS between δ and ϵ phases for ZrH_2 . The reduction in $N(\epsilon_F)$ about 0.5 states/eV unit cell per spin is strong while the FCC structure transforms to the FCT structure. We see that the high $N(\epsilon_F)$ splits to two picks near the Fermi level through the $\delta - \epsilon$ phase transition, and the system obtains structural stability in this way.

In Figure 10 we present the calculated phonon spectrum of ZrH_2 δ phase. It's clear to see that in the $\Gamma - K$, $\Gamma - X$, $\Gamma - L$ directions the Zr-character phonon modes have the imaginary frequencies around the Γ point. The imaginary phonon frequencies that the total energy of system can be decreased by a shift of atoms (here we can

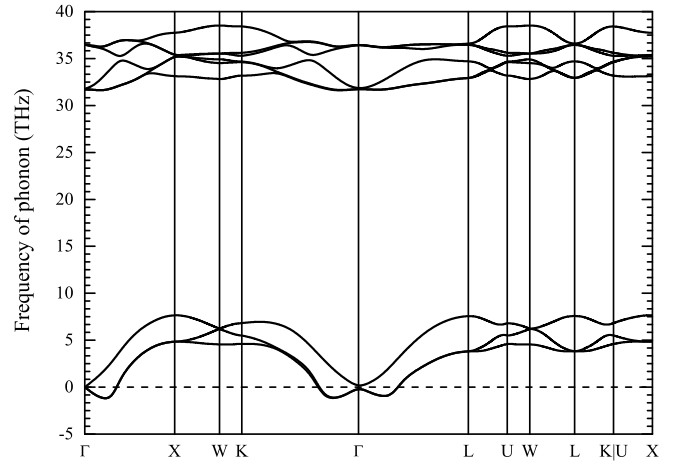


FIG. 10. The phonon spectrum of ZrH_2 δ phase.

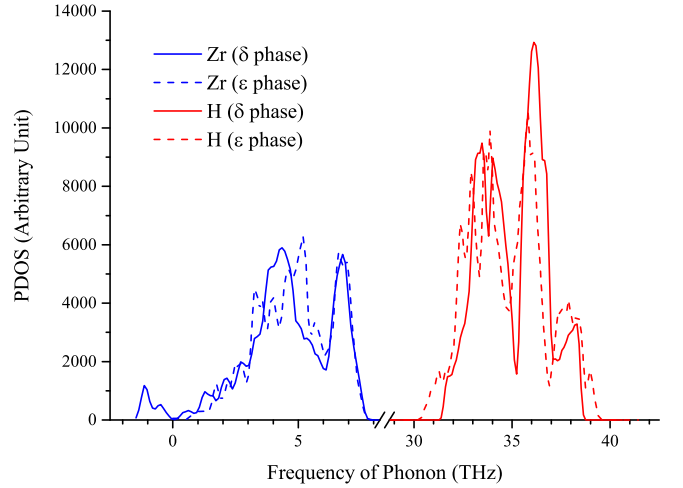


FIG. 11. The PDOS of ZrH_2 in δ and ϵ phases.

say density of electrons) in these three directions. As we said, through $\delta - \epsilon$ phase transition, the high $N(\epsilon_F)$ splits to two picks near the Fermi level, and the signs of electron band structure in the $\Gamma - K$, $\Gamma - X$, and $\Gamma - L$ directions also vanish. This explains why the imaginary phonon frequencies and signs of high $N(\epsilon_F)$ were observed in the same directions. It is also interesting to investigate the changes of phonon density of states (PDOS) through $\delta - \epsilon$ transition. As shown in Fig. 11, the frequency range of H-character optical phonon in δ phase is narrower than in ϵ phase, and the gap between acoustic and optical phonons 23.6 THz in δ phase is also narrower than 22 THz in ϵ phase. The picks in δ phase have a shift to the right (to the high frequency), for Zr-character phonon is 0.16 THz, and for H-character phonon is 0.5 THz. Also, the pick in δ phase at 36 THz is higher than in ϵ phase, it can be seen as a result of compressing the PDOS in ϵ phase. At a high symmetry condition (cubic structure), phonon modes in system have a higher degeneracy, which leads to the high pick and narrow range of H-character

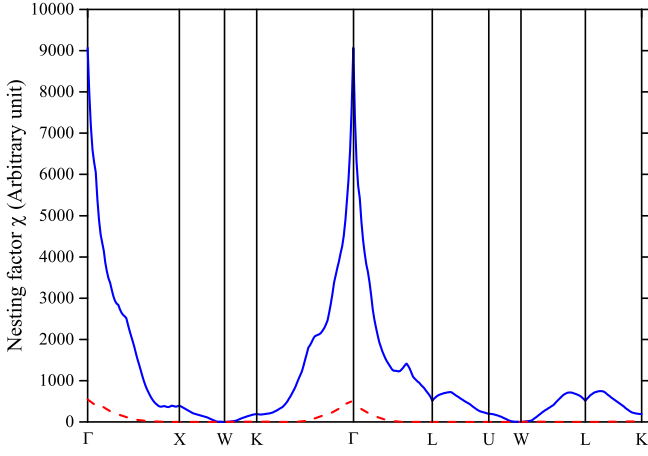


FIG. 12. The distribution of Fermi surface nesting factor along some high symmetry direction for ZrH₂. The blue solid line is Fermi surface nesting factor of δ phase, the red dash line represents Fermi surface nesting factor of ε phases.

optical phonon frequency, and it can be a reason why the H-character optical phonon plays a more important role in δ phase.

It should be pointed that the shape of PDOS and $\alpha^2 F(\omega)$ is similar, in fact, $\alpha^2 F(\omega)$ also can be seen as a modification of PDOS with a weight from electron-phonon coupling. The picks at phonon frequency of 6.5 THz and 35.5 THz are observed both in PDOS and $\alpha^2 F(\omega)$, but there are still differences. Through $\delta - \varepsilon$ phase transition, the pick at 6.5 THz doesn't change in PDOS, but reduces about 1 time in $\alpha^2 F(\omega)$; the pick at 35.5 THz reduces in both PDOS and $\alpha^2 F(\omega)$, but the reduction is stronger in $\alpha^2 F(\omega)$. This means that the electron background scattering plays a more important role in the change of electron-phonon coupling. It is also interesting to discuss the strong electron-phonon coupling in the range of imaginary phonon frequency of δ phase. In δ phase the main contribution on λ is from the range of imaginary phonon frequency, and the value is 1.016. The contribution on λ from the range of positive phonon frequency for δ phase is 0.868, which is the 4.57 times of the λ in ε phase.

As we said, the electron background scattering plays a important role in the globally strong electron-phonon coupling in δ phase. In particular, the connection between electronic background and electron-phonon interaction can be estimated by the Fermi surface nesting. We calculated the distribution of nesting factor $\chi(\mathbf{q}) = \sum_{m\mathbf{n}\mathbf{k}} \delta(\varepsilon_{n\mathbf{k}} - \varepsilon_F) \delta(\varepsilon_{m\mathbf{k}+\mathbf{q}} - \varepsilon_F)$ in reciprocal space for ZrH₂ as shown in Fig. 12. It is clear to see that for ZrH₂ δ phase the nesting is strong around Γ in the $\Gamma - K$, $\Gamma - X$, $\Gamma - L$ directions where the imaginary phonon frequencies appear. It is also found that the nesting factor has a maximum at Γ point. It is interesting that the Γ point is like a singular point that it is the center of imaginary phonon frequencies but the Zr-character acoustic phonon frequencies at Γ point are close to 0. The Zr-

character acoustic phonon modes are following the “2+1” splitting⁴², and frequencies of the two degenerate modes are imaginary, the frequencies of split mode is positive. This may be caused by that the nesting factor $\mathbf{q} \rightarrow 0$, and the Γ point as a point with the highest degeneracy cannot be modified, so that the period-lattice-distortion and the charge-density modulation have not been observed in ZrH₂, unfortunately. But the Fermi surface nesting behavior in ZrH₂ still can help us to understand the modification of electronic and phonon structure of system, especially the changes around Γ point. In particular, through $\delta - \varepsilon$ phase transition, the nesting factor χ not only strongly decreases around Γ point, but also has a global reduction. The reduction of nesting factor shows decreasing background scattering probability, which leads to the vanishing of the significant difference between $\alpha^2 F(\omega)$ and $\alpha_{tr}^2 F(\omega)$. The idea is simple that when the Fermi surface nesting is strong, many electrons at Fermi level don't have any change of energy and momentum after scattering with phonon. So that, the efficiency factor $\eta_{\mathbf{k},\mathbf{q}}^{m\nu}$ is small, and the value of λ_{tr} is much smaller than λ in δ phase. In particular, it can be seen that system defends the influence of electron-phonon coupling on electronic transport by modification of electronic structure in this way, the unphysical large electrical resistivity is reduced. Also, such a system with strong Fermi surface nesting is unstable, and it may lead to a phase transition.

In the end, we discuss the changes of electrical resistivity through tetragonal distortion of FCC lattice. In Figure 13 we present the calculated temperature dependence of electrical resistivity for ZrH₂ with different c/a ratio. It is clear to see that the electrical resistivity of ZrH₂ decreases through the tetragonal distortion. The electrical resistivity in δ phase is much larger than in ε phase, and the temperature dependence $\rho(T)$ in δ phase is steeper than in ε phase. It should be noticed that the results for the two states with ratio $c/a = 1$ and $c/a = 0.94$ are not physical, because of the imaginary phonon frequency. If we consider the Elishberg function $\alpha^2 F(\omega)$ and transport function $\alpha_{tr}^2 F(\omega)$, it's clear to see that through tetragonal distortion, the structural instability of system becomes more weak than δ phase, and the electron-phonon coupling is also going weaker. We conclude that the high electrical resistivity in δ phase is caused by its strong electron-phonon coupling, and it comes from the structural instability of FCC structure. We see that through the tetragonal distortion the unphysical imaginary phonon frequency and strong electron-phonon coupling are eliminated. As a result, the stable state of ε phase with a weak electron-phonon coupling strength is obtained, and it causes the reduction in electrical resistivity of ZrH_x system at a high hydrogen concentration ($x > 1.5$). In fact, the strong electron-phonon coupling in δ phase also can be seen as a result of its high N_F . The high N_F provides large number of backscattering electrons, and has a contribution on the strong Fermi surface nesting. Thus, we conclude that

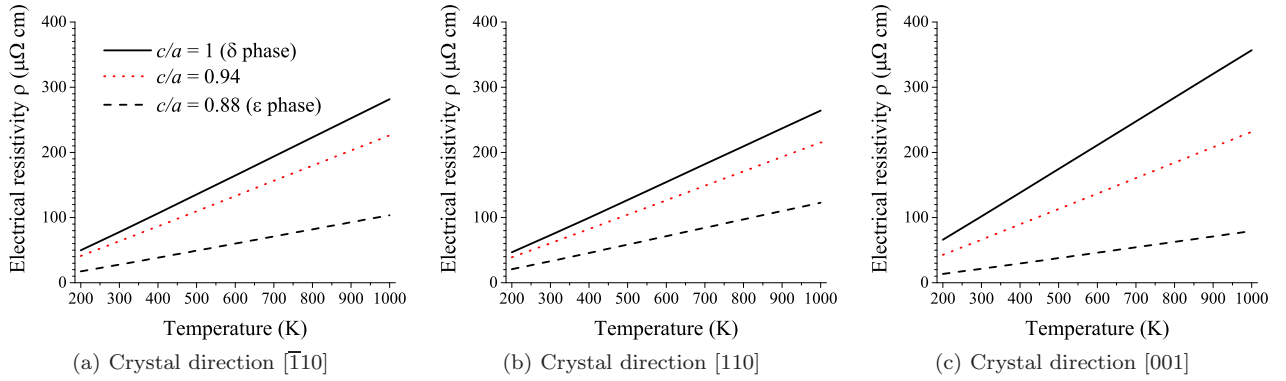


FIG. 13. A comparison of temperature dependence of electrical resistivity in ZrH_2 with various value of ratio c/a .

the strong electron-phonon coupling has a significant relevance with the structural instability of δ phase.

IV. SUMMARY AND CONCLUSIONS

We have presented a first-principles study of the electron-phonon coupling and electrical resistivity for Zr-H system. In present work, the systems $\text{ZrH}_{0.5}$, ZrH , $\text{ZrH}_{1.25}$, $\text{ZrH}_{1.5}$, $\text{ZrH}_{1.75}$, ZrH_2 and pure Zr were considered to clarify the H concentration dependence of physical properties for Zr-H system. The calculated results of electrical resistivity are in good agreement with experimental data, and the reduction in electrical resistivity at a high H concentration ($x > 1.5$) has been observed. We have obtained that at temperature 300 K the resistivity of ZrH_2 ($27.52 \mu\Omega \text{ cm}$) is smaller than pure Zr ($43.95 \mu\Omega \text{ cm}$), and the result is in good agreement with the experimental result where the resistivities of $42.6 \mu\Omega \text{ cm}$ for high purity Zr and $24.7 \mu\Omega \text{ cm}$ for $\text{ZrH}_{1.96}$ were obtained.

To explain the reduction, we have analyzed electron-

phonon coupling for Zr-H system by means of the Eliashberg function $\alpha^2 F(\omega)$ and Eliashberg transport function $\alpha_{tr}^2 F(\omega)$. The results show that with the increasing of H concentration in Zr, the change of electron-phonon coupling strength is not strong except in ZrH_2 . It has also been found that in the stable Zr-H system the difference between $\alpha^2 F(\omega)$ and $\alpha_{tr}^2 F(\omega)$ is small, but strong in δ phase of ZrH_2 . We have shown that the significant difference between $\alpha^2 F(\omega)$ and $\alpha_{tr}^2 F(\omega)$ in ZrH_2 δ phase is caused by the backscattering of electrons due to the strong Fermi surface nesting, and the strong Fermi surface nesting may be a reason why ZrH_2 system transforms from δ phase into ϵ phase. We have compared the calculated resistivity of ZrH_2 between δ and ϵ phases, and the result shows that the ZrH_2 δ phase has an extremely large resistivity due to the unphysical strong electron-phonon coupling which is related to the structural instability of δ phase. Though the tetragonal distortion, the unphysical imaginary phonon frequency and larger electron-phonon coupling constant λ are eliminated, and the ϵ phase of ZrH_2 with a weak electron-phonon coupling and low electrical resistivity is obtained.

* tan.tsichen@yandex.ru

- ¹ B. Sakintuna, F. Lamari-Darkrim, and M. Hirscher, *Int. J. Hydrog. Energy* **32**, 1121 (2007).
- ² W. M. Mueller, J. P. Blackledge, and G. G. Libowitz, *Metal hydrides* (Elsevier, 2013).
- ³ Y. Fukai, *The metal-hydrogen system: basic bulk properties*, Vol. 21 (Springer Science & Business Media, 2006).
- ⁴ C. Satterthwaite and I. Toepke, *Phys. Rev. Lett.* **25**, 741 (1970).
- ⁵ T. Skoskiewicz, *Phys. Status Solidi A* **11** (1972).
- ⁶ B. Geerken and R. Griessen, *J. Phys. F: Met. Phys.* **13**, 963 (1983).
- ⁷ Y. Sakamoto, K. Takai, I. Takashima, and M. Imada, *J. Phys.: Condens. Matter* **8**, 3399 (1996).
- ⁸ P. Bickel and T. Berlincourt, *Phys. Rev. B* **2**, 4807 (1970).
- ⁹ A. Zieliński and S. Sobieszczyk, *Int. J. Hydrog. Energy* **36**, 8619 (2011).
- ¹⁰ F. Wang and H. Gong, *Int. J. Hydrog. Energy* **37**, 12393 (2012).
- ¹¹ E. Zuzek, J. Abriata, A. San-Martin, and F. Manchester, *Bulletin of Alloy Phase Diagrams* **11**, 385 (1990).
- ¹² R. Khoda-Bakhsh and D. Ross, *J. Phys. F: Met. Phys.* **12**, 15 (1982).
- ¹³ P. Narang, G. Paul, and K. Taylor, *Journal of the Less Common Metals* **56**, 125 (1977).
- ¹⁴ Z. Zhao, J.-P. MORNIROLI, A. Legris, A. Ambar, Y. Khin, L. Legras, and M. BLAT-YRIEIX, *J. Microsc.* **232**, 410 (2008).
- ¹⁵ G. Ackland, *Phys. Rev. Lett.* **80**, 2233 (1998).
- ¹⁶ K. Niedźwiedź, B. Nowak, *et al.*, *J. Alloy. Compd.* **194**, 47 (1993).
- ¹⁷ J. S. Cantrell, R. J. Bowman, and D. Sullenger, *J. Phys. Chem.* **88**, 918 (1984).
- ¹⁸ R. Bowman Jr, E. Venturini, B. Craft, A. Attalla, and D. Sullenger, *Phys. Rev. B* **27**, 1474 (1983).
- ¹⁹ H. Yakel, *Acta Crystallogr.* **11**, 46 (1958).

- ²⁰ S. Kulkova, O. Muryzhnikova, and I. Naumov, *Phys. Solid State* **41**, 1763 (1999).
- ²¹ K. Miwa and A. Fukumoto, *Phys. Rev. B* **65**, 155114 (2002).
- ²² R. Quijano, R. de Coss, and D. J. Singh, *Phys. Rev. B* **80**, 184103 (2009).
- ²³ M. Gupta, *Phys. Rev. B* **25**, 1027 (1982).
- ²⁴ W. Wolf and P. Herzig, *J. Phys.: Condens. Matter* **12**, 4535 (2000).
- ²⁵ P. Zhang, B.-T. Wang, C.-H. He, and P. Zhang, *Comp. Mater. Sci.* **50**, 3297 (2011).
- ²⁶ F. Wang and H. Gong, *Int. J. Hydrog. Energy* **37**, 9688 (2012).
- ²⁷ R. Fletcher, N. Ho, and F. Manchester, *J. Phys. C: Solid State Phys.* **3**, S59 (1970).
- ²⁸ X. Gonze, F. Jollet, F. A. Araujo, D. Adams, B. Amadon, T. Applencourt, C. Audouze, J.-M. Beuken, J. Bieder, A. Bokhanchuk, *et al.*, *Comput. Phys. Commun.* **205**, 106 (2016).
- ²⁹ D. Hamann, *Phys. Rev. B* **88**, 085117 (2013).
- ³⁰ J. P. Perdew, K. Burke, and M. Ernzerhof, *Phys. Rev. Lett.* **77**, 3865 (1996).
- ³¹ M. Verstraete and X. Gonze, *Phys. Rev. B* **65**, 1 (2002).
- ³² R. Eitan, M. Mundt, and D. J. Tannor, *Phys. Rev. A* **83**, 053426 (2011).
- ³³ F. Giustino, *Rev. Mod. Phys.* **89**, 015003 (2017).
- ³⁴ P. B. Allen, *Phys. Rev. B* **6**, 2577 (1972).
- ³⁵ D. Zaharioudakis, *Comput. Phys. Commun.* **157**, 17 (2004).
- ³⁶ P. Allen, *Phys. Rev. B* **3**, 305 (1971).
- ³⁷ L. Schlapbach, *Hydrogen in Intermetallic Compounds I* (1988).
- ³⁸ C. Domain, R. Besson, and A. Legris, *Acta Mater.* **50**, 3513 (2002).
- ³⁹ P. D. Desai, H. M. James, and C. Y. Ho, *J. Phys. Chem. Ref. Data* **13**, 1097 (1984).
- ⁴⁰ S. Y. Savrasov and D. Y. Savrasov, *Phys. Rev. B* **54**, 16487 (1996).
- ⁴¹ V. H. Crespi and M. L. Cohen, *Solid State Commun.* **81**, 187 (1992).
- ⁴² P. Giannozzi, S. De Gironcoli, P. Pavone, and S. Baroni, *Phys. Rev. B* **43**, 7231 (1991).